Supporting Information

Highly selective generation of singlet oxygen from dioxygen with atomically dispersed catalysts

Wenjie Ma,[ac‡] Junjie Mao,[d‡] Chun-Ting He,[e‡] Leihou Shao,[a] Ji Liu,[a] Ming Wang,[ac] Ping Yu,[ac] Lanqun Mao[*ab]

[a] Beijing National Laboratory for Molecular Sciences, Key Laboratory of Analytical Chemistry for Living Biosystems, Institute of Chemistry, The Chinese Academy of Sciences (CAS), Beijing 100190, China

[b] College of Chemistry, Beijing Normal University, Xinjiekouwai Street 19, Beijing 100875, China

[c] University of Chinese Academy of Sciences, Beijing 100049, China

[d] Key Laboratory of Functional Molecular Solids, Ministry of Education, College of Chemistry and Materials Science, Anhui Normal University, Wuhu 241002, China

[e] MOE Key Laboratory of Functional Small Organic Molecule, College of Chemistry and Chemical Engineering, Jiangxi Normal University, Nanchang 330022, China

‡ These authors contributed equally to this work.

* Email: lqmao@bnu.edu.cn

Table of contents

S1-Experimental Section

1 Chemical Reagent

Iron acetylacetonate (Alfa Aesar), cobalt acetylacetonate (Alfa Aesar), copper acetylacetonate (Alfa Aesar), nickel acetylacetonate (Alfa Aesar), zinc nitrate hexahydrate (Alfa Aesar), 2-methylimidazole (Acros), methanol (Sinopharm Chemical), mannitol (Alfa Aesar), SOD (Sigma-Aldrich), NaN_3 (Sigma-Aldrich), 9,10-anthracenediyl-bis(methylene) dimalonic acid (Innochem), ρ-phthalic acid (Alfa Aesar), iodonitrotetrazolium chloride (Innochem), 5-tert-butoxycarbonyl-5-methyl-1-pyrroline N-oxide (BMPO, Dojindo), 2,2,6,6-tetramethylpiperidine (TEMP, Sigma-Aldrich), ascorbic acid (Sigma-Aldrich), fluorescein isothiocyanate (Sigma-Aldrich), 3-(4,5-dimethylthiazol-2-yl)-2,5-diphenyltetrazolium (Sigma-Aldrich), Calcein-AM (Sigma-Aldrich), propidium iodide (Sigma-Aldrich), and 2',7'-dichlorofluorescein diacetate (Sigma-Aldrich) were used without any further purification. DMEM, FBS and penicillin/streptomycin were purchased from Gibco (NY, USA). Britton-Robinson buffer (B-R buffer) was prepared by mixing 0.04 M H_3PO_4, HNO_3, H_3BO_3, and the pH values of the solutions were adjusted by 0.2 M NaOH. Aqueous solutions were all prepared with pure water obtained from a Milli-Q water system (Millipore, 18.2 MΩ cm). Unless stated otherwise, all experiments were carried out at room temperature.

2 Catalyst Preparation

M/ZIF-8 was synthesized via in-situ encapsulation of metal acetylacetonate in the cage of ZIF-8. Typically, 1.68 g $Zn(NO_3)\cdot 6H_2O$ and 3.70 g 2-methylimidazole were dissolved in 50 mL methanol, respectively. Metal acetylacetonate (0.20 g for iron acetylacetonate and cobalt acetylacetonate, 0.15 g for copper acetylacetonate and nickel acetylacetonate) was dissolved in the methanolic solution of $Zn(NO_3)_2$. Then, two solutions were mixed and stirred for 24 h at room temperature. The precipitates were collected by centrifugation, washed with methanol for several times, and finally dried at 80 °C under vacuum for 12 h to obtain M/ZIF-8. For the preparation of core-shell M/ZIF-8@TA, 200 mg of the as-prepared M/ZIF-8 was first dispersed in 50 mL water. An aqueous solution of tannic acid (500 mg in 50 mL water) was quickly poured into M/ZIF-8 dispersion. After standing for 5 minutes, the mixture was centrifuged, washed with water for several times and dried at 80 °C under vacuum for 12 h to get M/ZIF-8@TA precursors. Finally, M/ZIF-8@TA was put into a ceramic boat, placed in a tube furnace, and heated to 900 °C with a heating rate of 3 $°C\cdot min^{-1}$ and kept at 900 °C for 3 h under flowing Ar gas (99.999%). The black powder of M_1/HNC SACs was obtained after the carbonization process.

3 Catalyst Characterization

3.1 Instruments

PXRD patterns were performed on X-ray powder diffractometer (Empyrean, PANalytical) with Cu Kα radiation (λ = 1.5406 Å). Raman spectra were recorded on Raman spectrometer (LabRAM HR Evolution, HORIBA) with the 532 nm line of an Argon ion laser as the excitation source. TEM images and high-resolution TEM images were obtained on transmission electron microscope (JEM-2100F, JEOL) operated at 200kV. HAADF-STEM images were carried out by aberration-corrected scanning transmission electron microscope (Titan 80-300, FEI) operated at 300 kV. XAFS spectra were collected at 1W1B station in Beijing Synchrotron Radiation Facility (BSRF). The storage rings of BSRF were conducted at 2.5 GeV with a maximum current of 250 mA. The data was collected with a Si(111) double-crystal monochromator in transmission mode using ionization chamber for the references, and in fluorescence excitation mode using Lytle detector for M_1/HNC. All spectra were obtained under ambient conditions. ICP-OES data were obtained using ICP-OES analyzer (725-ES, Agilent) calibrated with standard solution.

3.2 XAFS Analysis

The collected EXAFS data were processed according to the standard procedures using the ATHENA module implemented in the IFEFFIT software packages. The k^3-weighted EXAFS spectra were acquired by subtracting the post-edge background from the overall absorption and then normalizing with respect to the edge-jump step. Subsequently, k^3-weighted $\chi(k)$ data of Fe K-edge were Fourier transformed to real (R) space using a hanning windows (dk=1.0 $Å^{-1}$) to separate the EXAFS contributions from different coordination shells. To obtain the quantitative structural parameters around central atoms, least-squares curve parameter fitting was conducted using the ARTEMIS module of IFEFFIT software packages. The following EXAFS equation was used:

$$\chi(k) = \sum_j \frac{N_j S_0^2 F_j(k)}{kR_j^2} exp[-2k^2\sigma_j^2] exp[\frac{-2R_j}{\lambda(k)}] \sin[2kR_j + \phi_j(k)]$$

S_0^2 is the amplitude reduction factor, $F_j(k)$ is the effective curved-wave backscattering amplitude, N_j is the number of neighbors in the j^{th} atomic shell, R_j is the distance between the X-ray absorbing central atom and the atoms in the j^{th} atomic shell (backscatterer), λ is the mean free path in Å, $\phi_j(k)$ is the phase shift (including the phase shift for each shell and the total central atom phase shift), σ_j is the Debye-Waller parameter of the j^{th} atomic shell (variation of distances around the average R_j). The functions $F_j(k)$, λ and $\phi_j(k)$ were calculated with the ab initio code FEFF8.2.

4 Selective $^1O_2$ Generation

4.1 TMB Oxidation Reaction

The catalytic activity toward TMB oxidation was verified by determining the characteristic absorbance of ox-TMB at 652 nm using a Synergy H1M microplate reader (BioTek, USA). In brief, different concentration of M_1/HNC or HNC (0-5 μg/mL) was added to a solution of 0.5 mM TMB in B-R buffer at different pH values, and the absorbance was immediately recorded at different reaction times. TMB oxidation with different scavengers (NaN_3, 2.5 mM; mannite, 2.5 mM; SOD, 200 unit/mL) were conducted to identify the generated ROS.

4.2 Monitoring Selective Generation of $^1O_2$ with M_1/HNC

The catalytic performances of $^1O_2$ generation of M_1/HNC SACs were measured by the oxidation of ABDA using a Synergy H1M microplate reader (BioTek, USA). Briefly, different concentration of M_1/HNC or HNC (0-5 μg/mL) was added to a solution of 20 μM ABDA in B-R buffer at different pH values, and the fluorescent intensity ($\lambda_{ex}/\lambda_{em}$ = 380/433 nm) was immediately recorded at different reaction times. The kinetic constants (k values) were estimated by the pseudo-first-order equation:

$$\ln (F_0/F) = kt$$

where, t is the reaction time, F_0 and F stand for fluorescent intensity of ABDA at initial stage and at the time of t, respectively, and k is the pseudo-first-order kinetic constant.

The single-site kinetic constants ($k_{single\text{-}site}$ values) were obtained according to the following equation:

$$k_{single\text{-}site} = kM/(m \cdot wt\%)$$

where, k is the apparent constant rate, M stands for relative atomic mass, m is mass of catalyst (1 μg) used in the ABDA oxidation, and $wt\%$ is the metal content of the catalyst determined by ICP-OES.

4.3 EPR Spectroscopy

EPR measurements were conducted using Brucker model EPR 300E spectrometer equipped with a Quanta-Ray Nd:YAG laser (532 nm). The quartz capillary tube was used to minimize experimental errors. In a typical measurement, 20 μg/mL Fe_1/HNC was added to a mixture of 50 mM TEMP in B-R buffer solution (pH 4.0). EPR spectrum was recorded after 1.5 min of mixing. The EPR measurements for O_2^- and •OH were also performed as described above, except the use of BMPO (25 mM) as the spin-trapping agent.

5 DFT Calculations

All the geometry optimizations and energy relaxation were performed by spin-polarized plane-wave DFT, which was implemented in CASTEP program. The periodical models were built up based on a

6 × 6 supercell of graphene. A vacuum slab of 18 Å was introduced to avoid interactions between periodic images. The exchange-correlation functional of Perdew-Burke-Ernzerhof (PBE) within the generalized gradient approximation (GGA) and the ultrasoft pseudopotentials were adopted. The cutoff energy of 571 eV was chosen for the plane-wave basis. The convergence criteria for the total energy, stress, forces, atomic displacement, and SCF iterations were set as 1×10^{-5} eV/atom, 5×10^{-2} GPa, 3×10^{-2} eV/Å, 1×10^{-3} Å, and 1×10^{-6} eV/atom, respectively.

6 *In vitro* and *in vivo* Inhibition of Tumor Cell Proliferation

6.1 Cell Culture

HeLa cells were purchased from National Infrastructure of Cell Line Resource (China) and maintained in high-glucose Dulbecco's modified eagle medium (DMEM) supplemented with 10% fetal bovine serum (FBS) and 1% penicillin/streptomycin at 37 °C under the atmosphere of 5% CO_2. For the intracellular delivery, HeLa cells were sub-cultured and seeded in 48-well plates for 24 h prior to experiment.

6.2 Cellular Internalization of Fe_1/HNC *in vitro*

To enhance the dispersibility and biocompatibility of Fe_1/HNC, DSPE-PEG2000 was used to PEGylate Fe_1/HNC with a mass ratio of 5:1 through hydrophobic interaction under intensive sonication. The PEGylated Fe_1/HNC (P-Fe_1/HNC) loaded with FITC was used to visualize the cellular uptake. HeLa cells were initially seeded at a density of 1.5×10^5 cells in glass bottom cell culture dish for 24 h, and then treated with P-Fe_1HNC at 0.1 mg/mL for 6 h at 37 °C. After incubation, the cells were washed thoroughly with Dulbecco's phosphate-buffered saline (DPBS) twice, followed by CLSM imaging on OLYMPUS FV1000-IX81.

6.3 Cell Viability Investigation

HeLa cells were initially seeded at a density of 1.5×10^{-5} cells in glass bottom cell culture dish for 24 h, and then treated with different concentration of P-HNC or P-Fe_1HNC from 0 to 0.3 mg/mL for 12 h at 37 °C. After incubation, the cells were washed thoroughly with DPBS twice, followed by a standard MTT assay. Control experiment using P-HNC was conducted with the same procedure to Fe_1/HNC treatment. The cell viability was further investigated by using Calcein-AM and PI to stain viable cells and dead cells, respectively. Briefly, HeLa cells were initially seeded in glass bottom cell culture dish at a density of 5×10^4, and then treated with 0.1 mg/mL P-Fe_1/HNC overnight. At the end of incubation, the cells were harvested and washed with DPBS, followed by Calcein-AM (2 μM) and PI (4.5 μM) co-

staining for 30 min, and subjected to CLSM imaging. Control experiment using P-HNC was carried out with the same procedure to Fe_1/HNC treatment.

6.4 Intracellular ROS Imaging

The intracellular ROS levels of HeLa cells with P-Fe_1/HNC treatment were imaged with 2',7'-dichlorofluorescein diacetate (DCFH-DA) staining. HeLa cells were initially seeded in glass bottom cell culture dish at a density of 5×10^4, and then treated with 0.1 mg/mL P-Fe_1/HNC overnight. At the end of incubation, the cells were harvested and washed with DPBS, followed by DCFH-DA (10 μM) staining for 30 min, and subjected to CLSM imaging. Control experiment using P-HNC was carried out with the same procedure to Fe_1/HNC treatment.

6.5 Inhibition of Tumor Cell Proliferation with Fe_1/HNC SAC *in vivo*

All the animal experiments were conducted with the guidelines of the Animal Advisory Committee at the State Key Laboratory of Cognitive Neuroscience and Learning, and were approved by the Institutional Animal Care and Use Committee at Beijing Normal University. HeLa cells (1×10^7 cells) were subcutaneously injected to the left axilla region of female BALB/c nude mice (4-6 weeks old) to establish the HeLa xenograft tumor model. When the tumor volumes reached about 100 mm^3, the mice were randomly assigned to three groups and intravenously injected with PBS, P-HNC, and P-Fe_1/HNC every other day for five times, respectively. The tumor volume (V) was calculated by the following formula: $V = d_1 \times d_2^2$, where d_1 and d_2 represent the tumor length and tumor width, respectively. The tumor volume and body weight were monitored every other day. At the end of the experiment, all mice were sacrificed. Tumor tissues were weighted and blood samples were collected for the biosafety analysis.

S2-Supplementary figures and tables

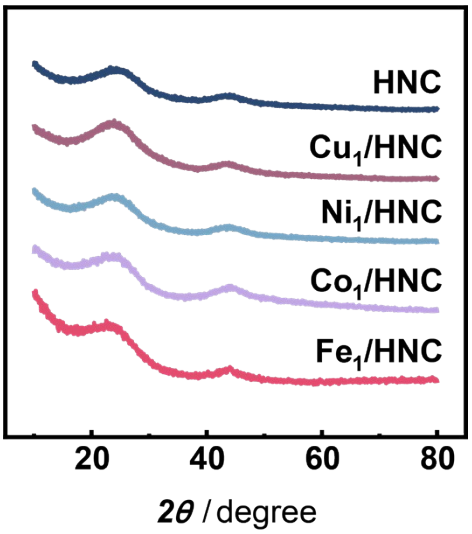

Fig. S1 XRD patterns of M_1/HNC SACs and HNC.

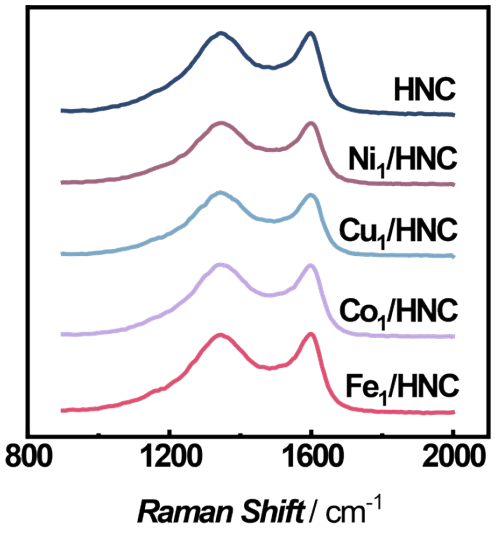

Fig. S2 Raman spectra of M_1/HNC SACs and HNC.

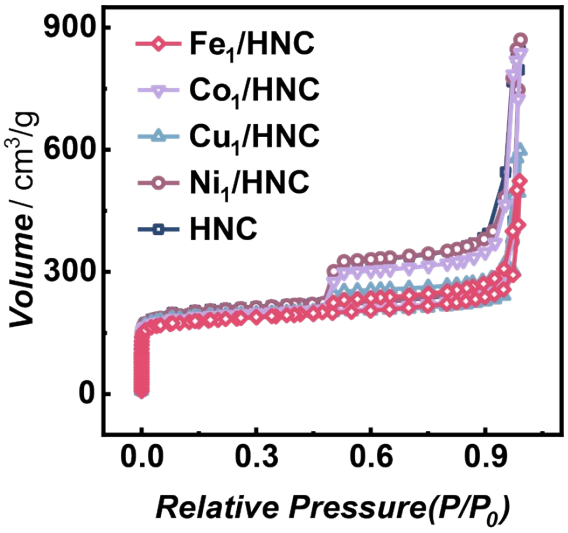

Fig. S3 Nitrogen sorption isotherms of M_1/HNC and HNC.

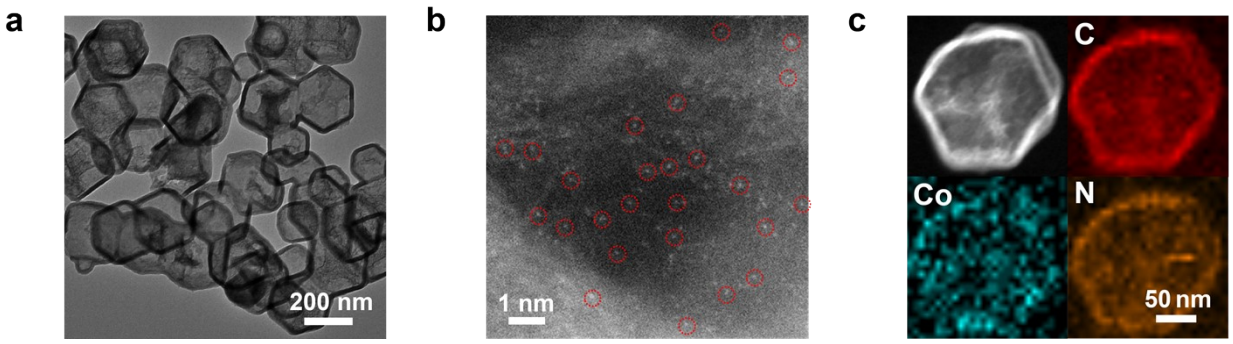

Fig. S4 (a) TEM image of Co_1/HNC. (b) Aberration-corrected HAADF-STEM image of Co_1/HNC showing atomically dispersed Co atoms as bright dots highlighted with red circles. (c) HAADF-STEM image and corresponding elemental mapping images of Co_1/HNC (C, red; Co, green; N, orange).

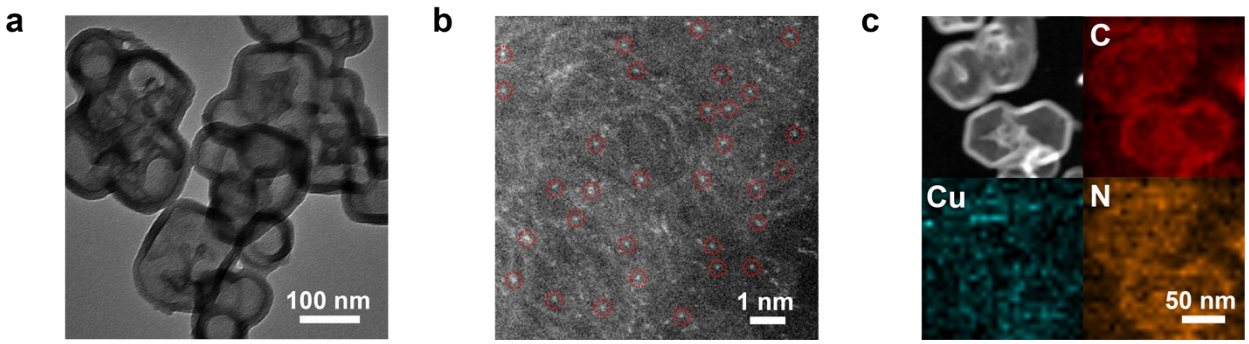

Fig. S5 (a) TEM image of Cu_1/HNC. (b) Aberration-corrected HAADF-STEM image of Cu_1/HNC showing atomically dispersed Cu atoms as bright dots highlighted with red circles. (c) HAADF-STEM image and corresponding elemental mapping images of Cu_1/HNC (C, red; Cu, green; N, orange).

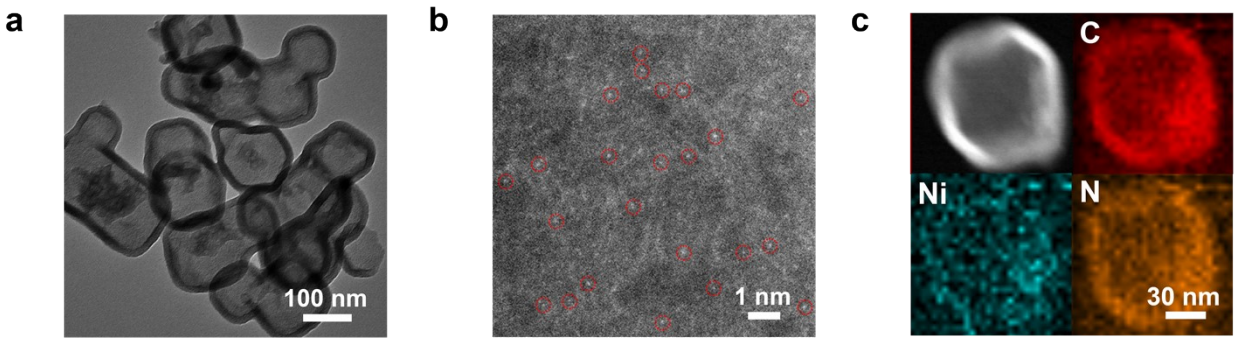

Fig. S6 (a) TEM image of Ni_1/HNC. (b) Aberration-corrected HAADF-STEM image of Ni $_1$/HNC showing atomically dispersed Ni atoms as bright dots highlighted with red circles. (c) HAADF-STEM image and corresponding elemental mapping images of Ni $_1$/HNC (C, red; Ni, green; N, orange).

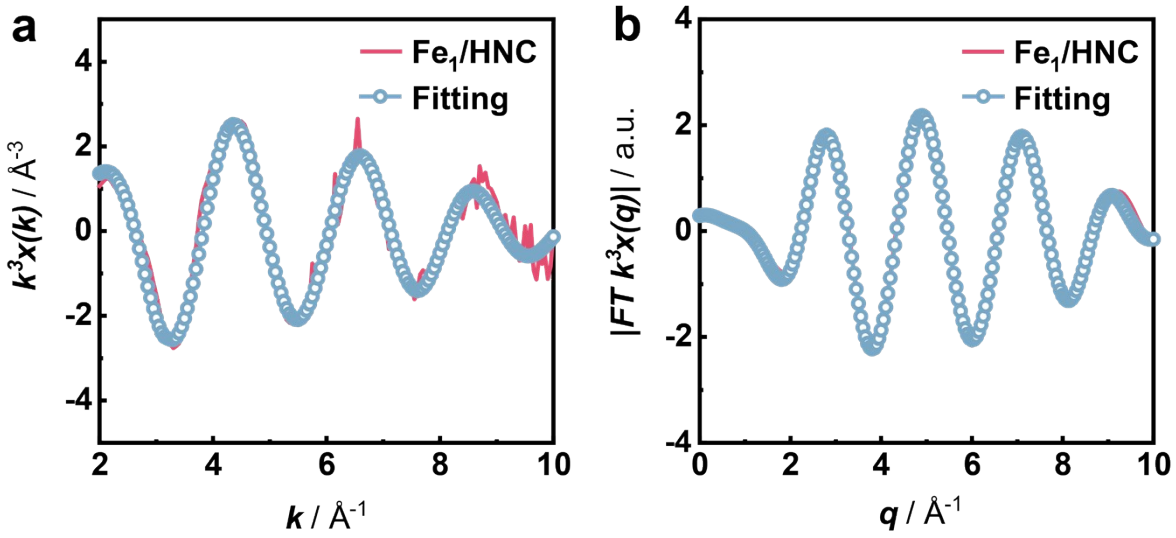

Fig. S7 Fourier-transformed EXAFS spectrum and corresponding fitting curve of Fe_1/HNC in (a) *k*-space and (b) *q*-space.

Table S1.. Structural parameters extracted from the Fe K-edge EXAFS fitting. (S_0^2 = 0.78)

sample	Scattering pair	CN	R(Å)	$\sigma^2(10^{-3}Å^2)$	ΔE_0(eV)	R factor
Fe_1/HNC	Fe-N	4.15	2.02	11.5	0.4	0.01
Fe foil	Fe-Fe1	8*	2.45	6.1	4.5	0.007
	Fe-Fe2	6*	2.84	7.7		

S_0^2 is the amplitude reduction factor; CN is the coordination number; R is interatomic distance (the bond length between central atoms and surrounding coordination atoms); σ^2 is Debye-Waller factor (a measure of thermal and static disorder in absorber-scatterer distances); ΔE_0 is edge-energy shift (the difference between the zero kinetic energy value of the sample and that of the theoretical model). R factor is used to value the goodness of the fitting.

* This value was fixed during EXAFS fitting, based on the known structure.

Error bounds that characterize the structural parameters obtained by EXAFS spectroscopy were estimated as N ± 20%; R ± 1%; σ^2 ± 20%; ΔE_0 ± 10%.

Fe_1HNC (FT range: 2.0-12.0 $Å^{-1}$; fitting range: 1.1-2.8 Å)

Fe foil (FT range: 2.0-12.0 $Å^{-1}$; fitting range: 1.3-3 Å)

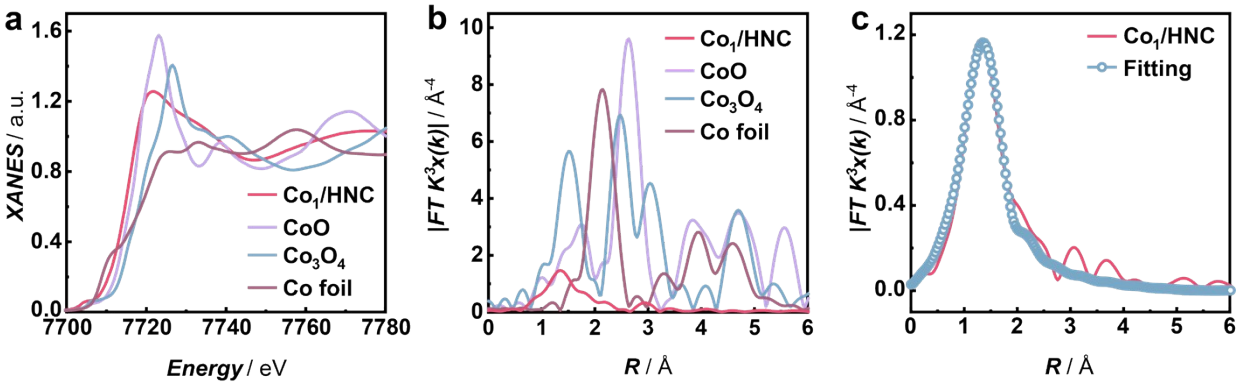

Fig. S8 (a) Normalized XANES spectra and (b) corresponding Fourier-transformed spectra at Co K-edge of Co_1/HNC (red line), CoO (purple line), Co_3O_4 (blue line), and Co foil (brown line). (c) Fourier-transformed EXAFS spectrum and corresponding fitting curve of Co_1/HNC in *R*-space.

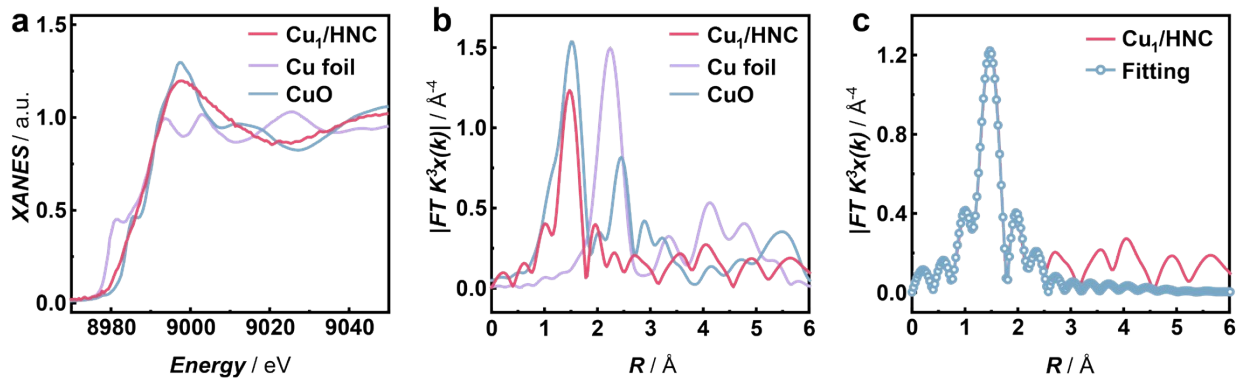

Fig. S9 (a) Normalized XANES spectra and (b) corresponding Fourier-transformed spectra at Cu K-edge of Cu_1/HNC (red line), Cu foil (purple line), and CuO (blue line). (c) Fourier-transformed EXAFS spectrum and corresponding fitting curve of Cu_1/HNC in *R*-space.

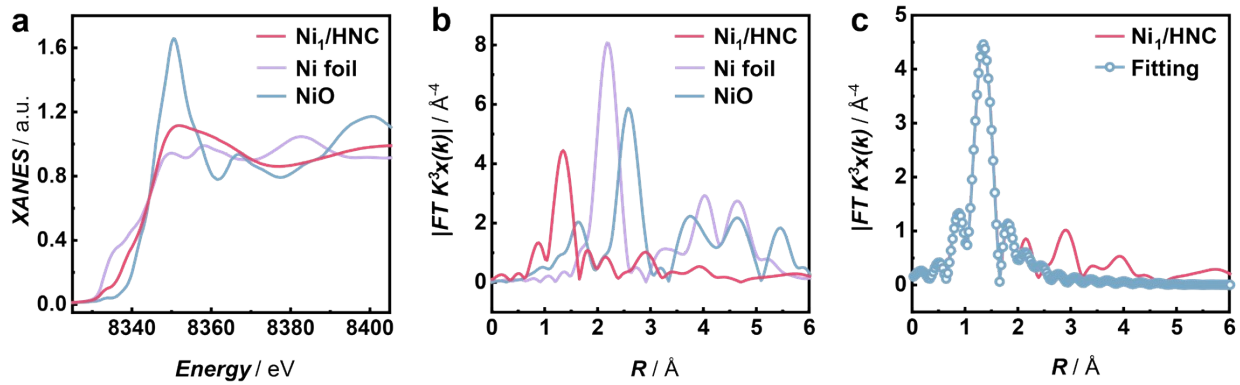

Fig. S10 (a) Normalized XANES spectra and (b) corresponding Fourier-transformed spectra at Ni K-edge of Ni_1/HNC (red line), Ni foil (purple line), and NiO (blue line). (c) Fourier-transformed EXAFS spectrum and corresponding fitting curve of Ni_1/HNC in *R*-space.

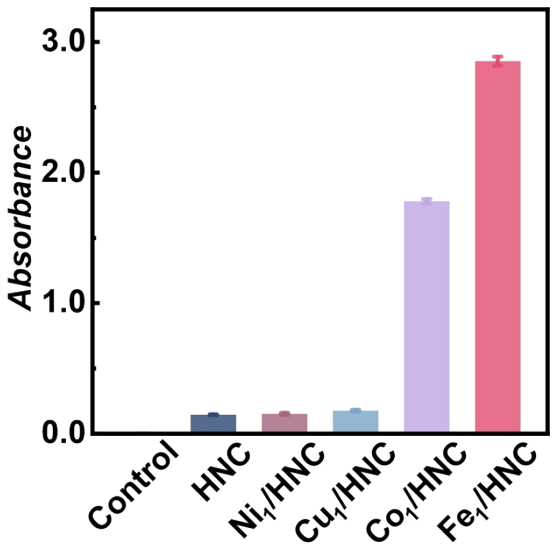

Fig. S11 The absorbance at 20 min of ox-TMB monitored at 652 nm for the catalytic oxidation by 5 μg/mL M_1/HNC and HNC in B-R buffer (pH 4.0).

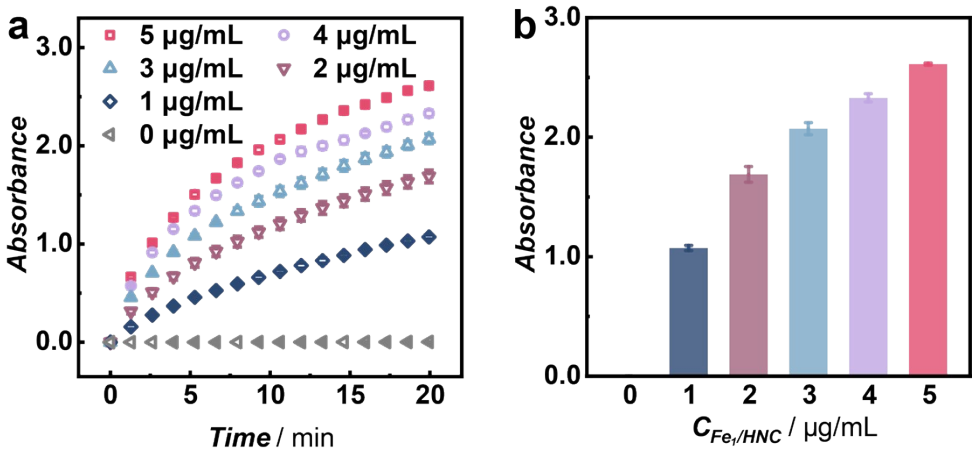

Fig. S12 (a) Time-dependent absorbance changes and (b) the absorbance at 20 min of ox-TMB monitored at 652 nm for the catalytic oxidation by Fe_1/HNC with different concentrations in B-R buffer (pH 4.0).

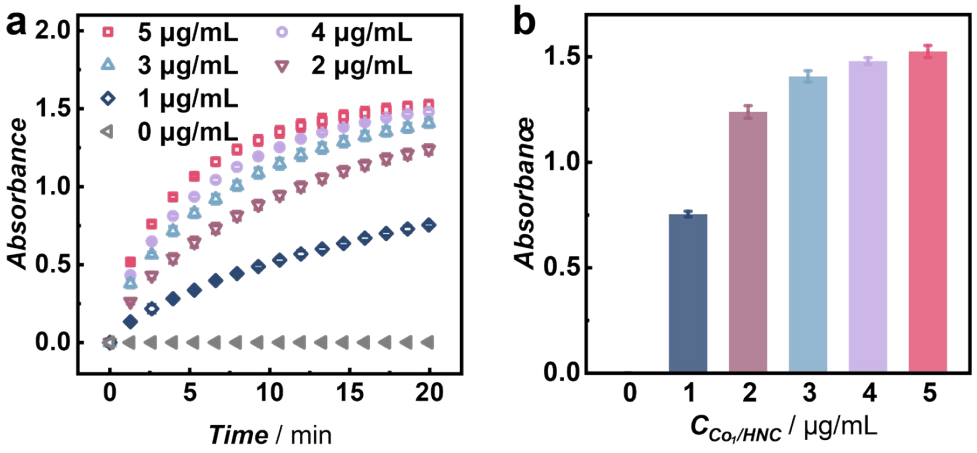

Fig. S13 (a) Time-dependent absorbance changes and (b) the absorbance at 20 min of ox-TMB monitored at 652 nm for the catalytic oxidation by Co_1/HNC with different concentrations in B-R buffer (pH 4.0).

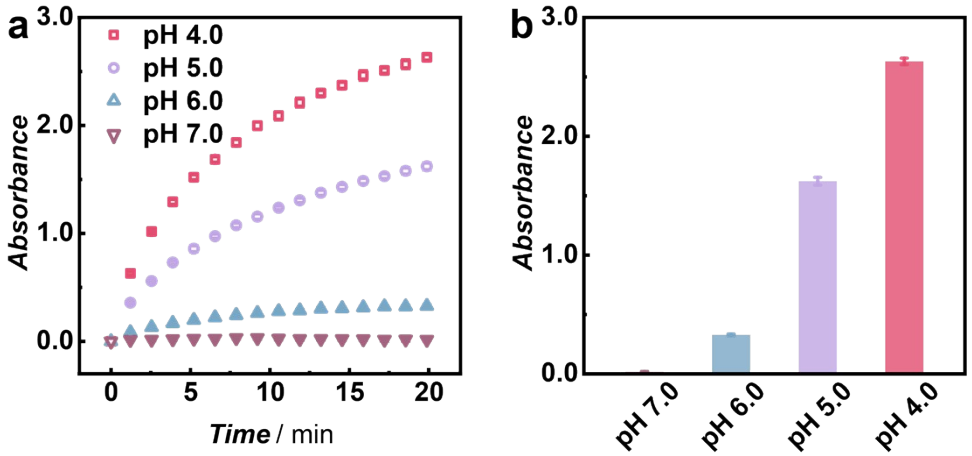

Fig. S14 (a) Time-dependent absorbance changes and (b) the absorbance at 20 min of ox-TMB monitored at 652 nm for the catalytic oxidation by 5 μg/mL Fe_1/HNC in B-R buffer with different pH values.

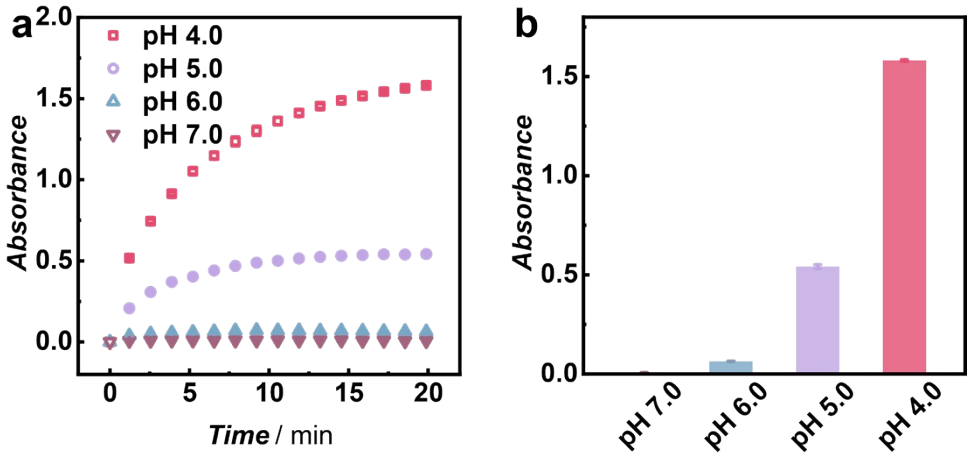

Fig. S15 (a) Time-dependent absorbance changes and (b) the absorbance at 20 min of ox-TMB monitored at 652 nm for the catalytic oxidation by 5 μg/mL Co_1/HNC in B-R buffer with different pH values.

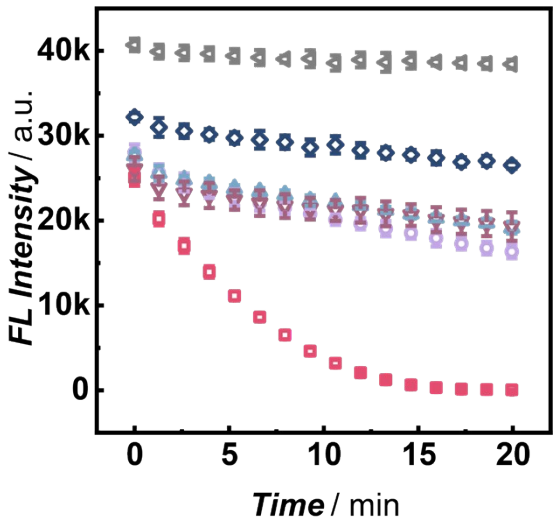

Fig. S16 Time-dependent fluorescence intensity changes of ABDA monitored at $\lambda_{ex}/\lambda_{em}$ = 380/433 nm) for the catalytic oxidation with 5 μg/mL Fe_1/HNC (red line), Co_1/HNC (purple line), Cu_1/HNC (blue line), Ni_1/HNC (brown line), HNC (dark blue line) and without catalyst (gray line) in B-R buffer (pH 4.0).

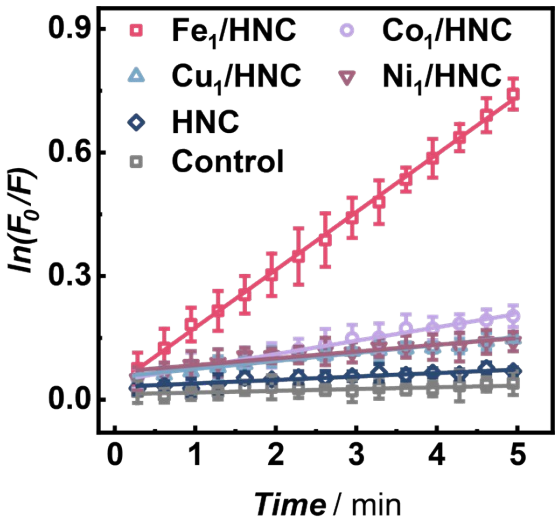

Fig. S17 First-order kinetics curves of ABDA oxidation catalyzed by M_1/HNC SACs and HNC.

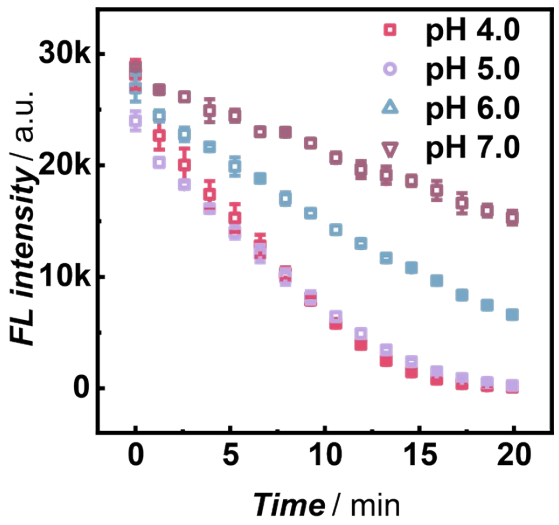

Fig. S18 Time-dependent fluorescence intensity changes of ABDA monitored at $\lambda_{ex}/\lambda_{em}$ = 380/433 nm for the catalytic oxidation by 5 μg/mL Fe_1/HNC in B-R buffer with different pH values.

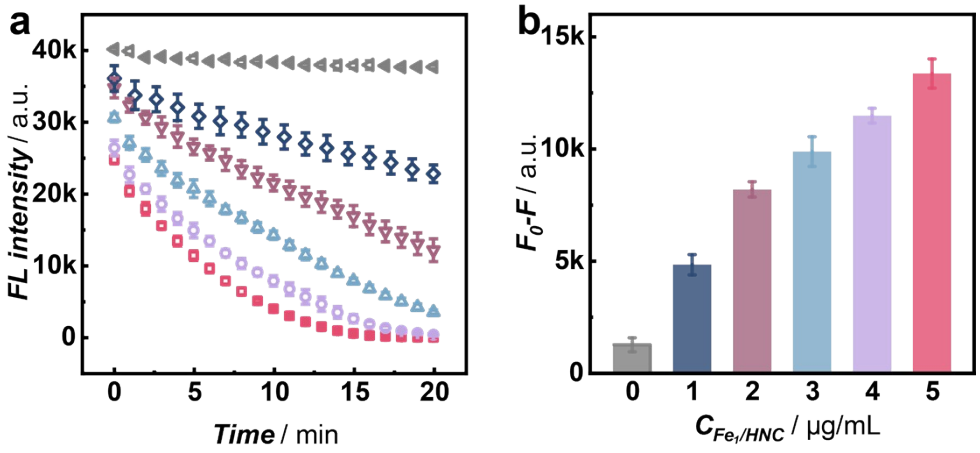

Fig. S19 (a) Time-dependent fluorescence intensity changes and (b) the fluorescence intensity at 5 min of ABDA monitored at $\lambda_{ex}/\lambda_{em}$ = 380/433 nm for the catalytic oxidation by Fe_1/HNC with the concentration of 5 μg/mL (red line), 4 μg/mL (purple line), 3 μg/mL (blue line), 2 μg/mL (brown line), 1 μg/mL (dark blue line) and without catalyst (gray line) in B-R buffer (pH 4.0).

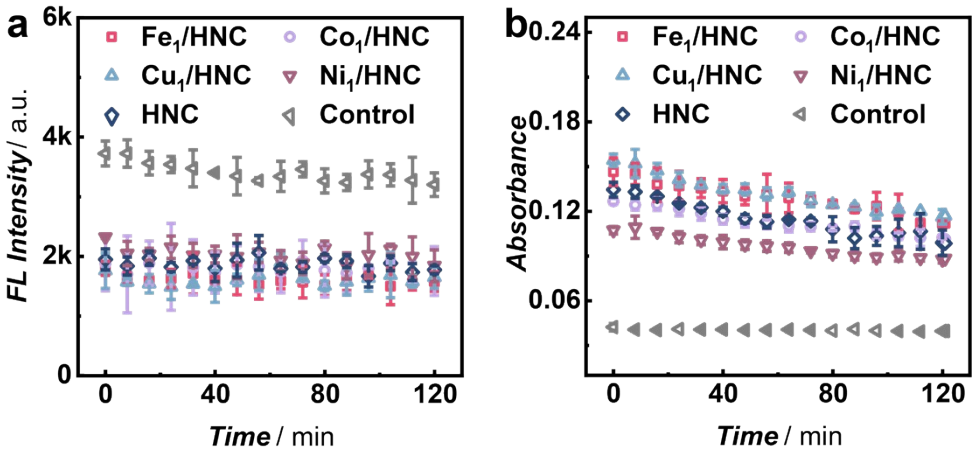

Fig. S20 (a) Time-dependent fluorescence intensity changes of PTA monitored at $\lambda_{ex}/\lambda_{em}$ = 315/400 nm for the catalytic oxidation by 5 μg/mL M_1/HNC and HNC in B-R buffer (pH 4.0). (b) Time-dependent absorbance changes of INT monitored at 510 nm for the catalytic oxidation by 5 μg/mL M_1/HNC and HNC in B-R buffer (pH 4.0).

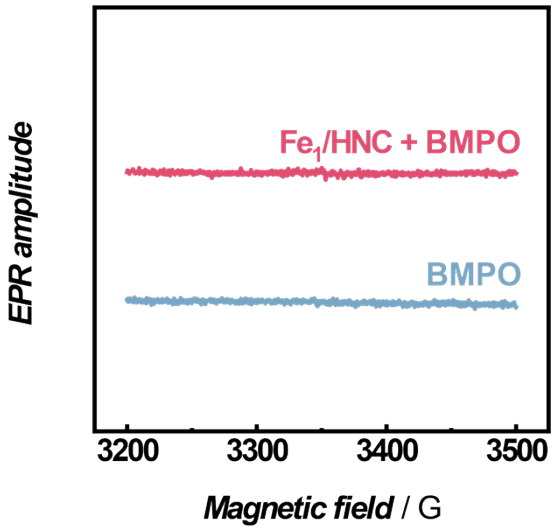

Fig. S21 BMPO ESR signals in the absence (blue line) and presence of 20 μg/mL Fe_1/HNC in B-R buffer (pH 4.0).

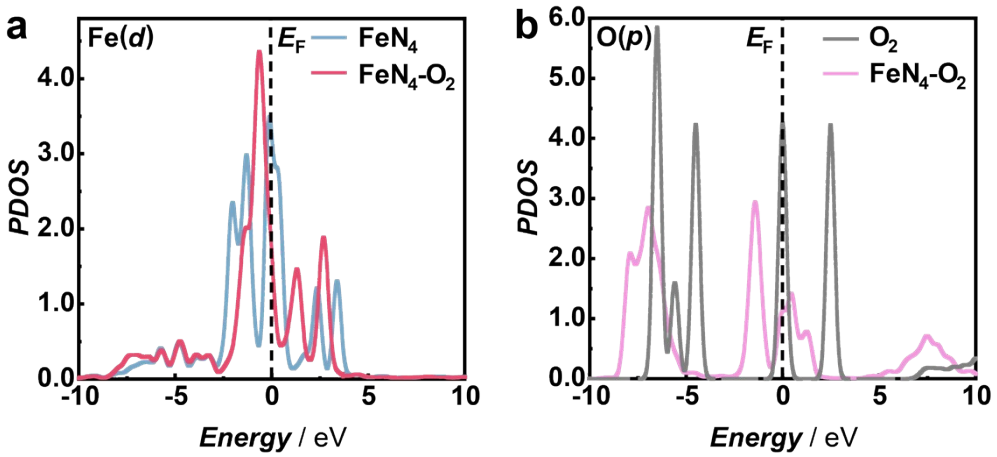

Fig. S22 (a) PDOS for the Fe 3d orbital of FeN_4 site before (blue) and after (red) adsorption of O_2. (b) PDOS for the O 2p orbital of O_2 in state free (gray line) and upon chemisorption on FeN_4 site (pink line).

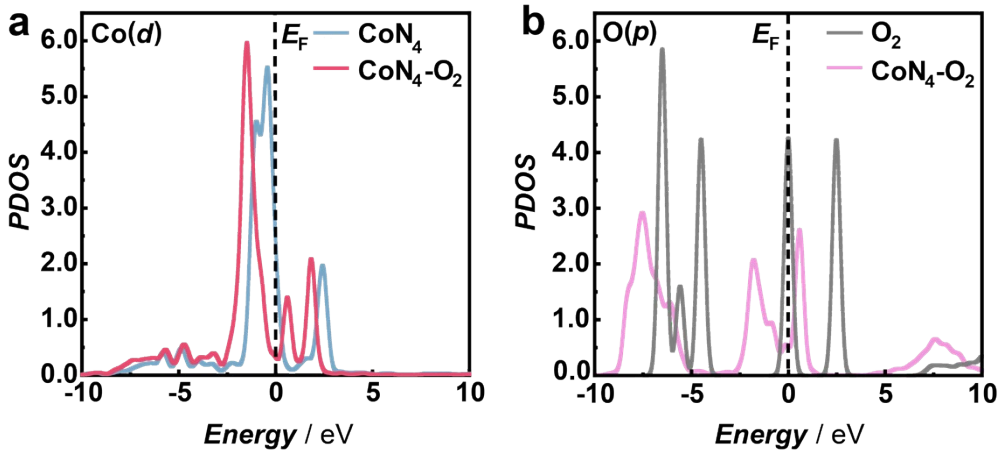

Fig. S23 (a) PDOS for the Co 3d orbital of CoN_4 site before (blue) and after (red) adsorption of O_2. (b) PDOS for the O 2p orbital of O_2 in state free (gray line) and upon chemisorption on CoN_4 site (pink line).

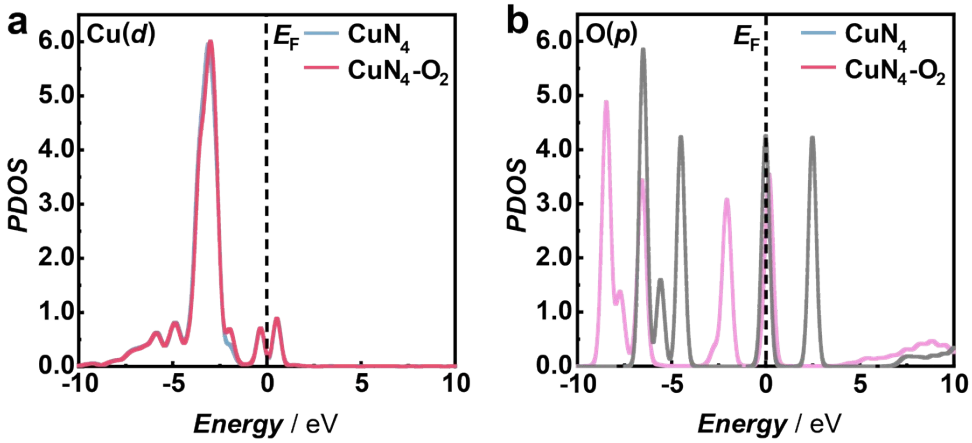

Fig. S24 (a) PDOS for the Cu 3d orbital of CuN_4 site before (blue) and after (red) adsorption of O_2. (b) PDOS for the O 2p orbital of O_2 in state free (gray line) and upon chemisorption on CuN_4 site (pink line).

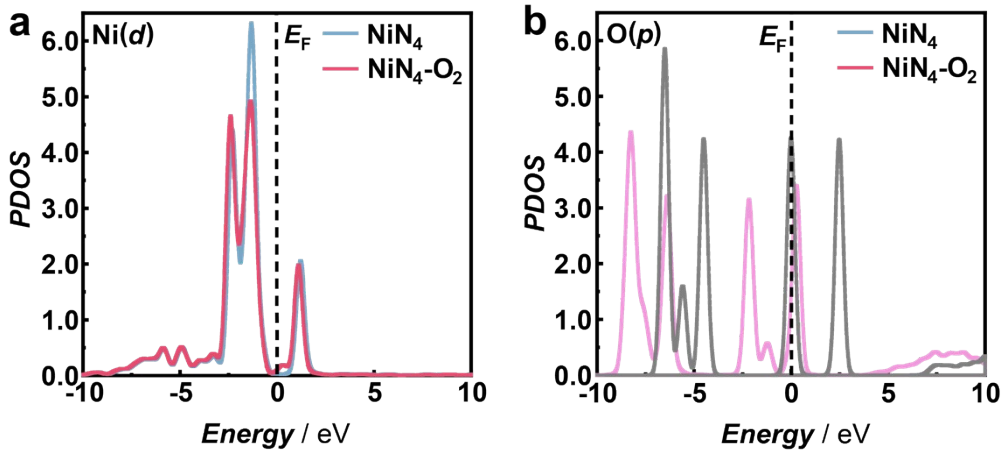

Fig. S25 (a) PDOS for the Ni 3d orbital of NiN_4 site before (blue) and after (red) adsorption of O_2. (b) PDOS for the O 2p orbital of O_2 in state free (gray line) and upon chemisorption on NiN_4 site (pink line).

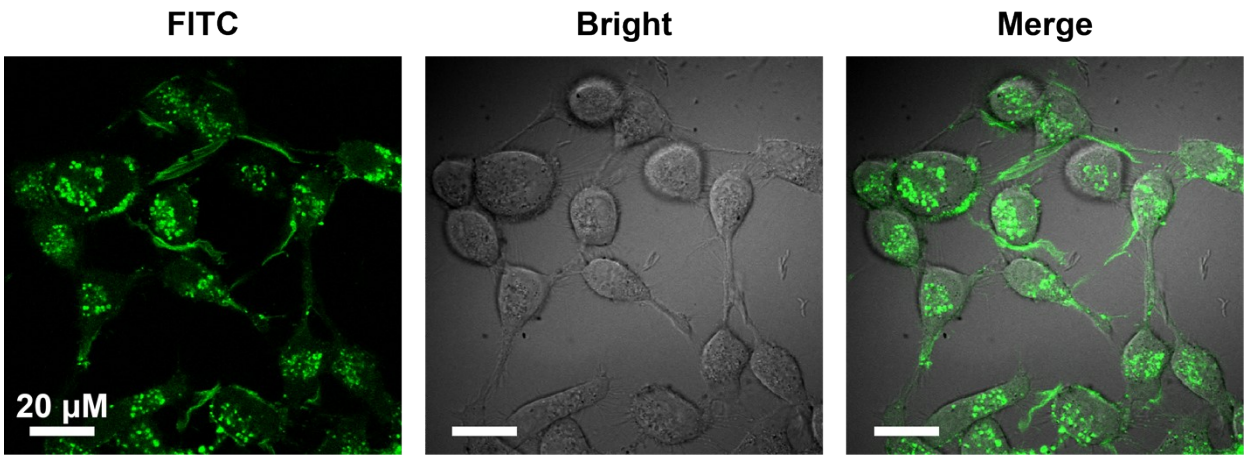

Fig. S26 CLSM images of HeLa cells treated with FITC-loaded P-Fe_1/HNC for 6 h.

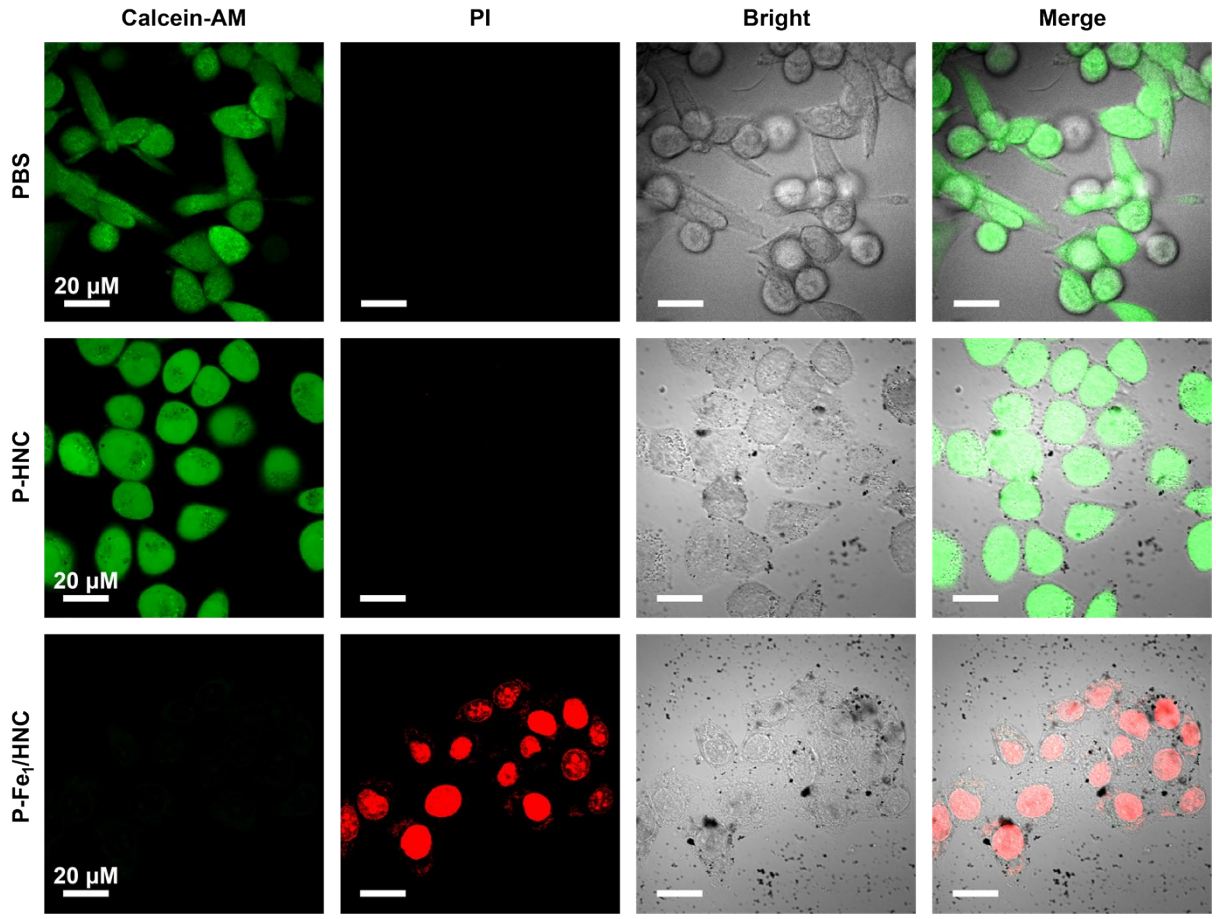

Fig. S27 CLSM images of HeLa cells co-stained with Calcein-AM and PI after the treatment with PBS, P-HNC and P-Fe_1/HNC, respectively.

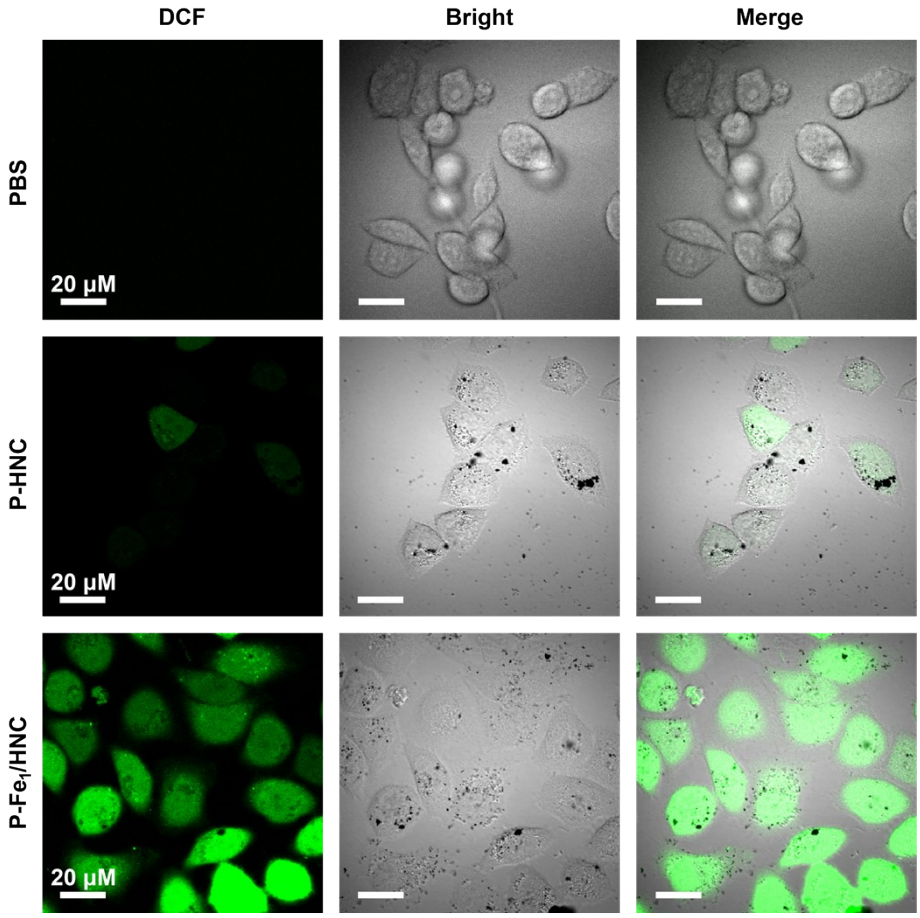

Fig. S28 CLSM images of HeLa cells stained with DCFH-DA after the treatment with PBS, P-HNC and P-Fe_1/HNC, respectively.

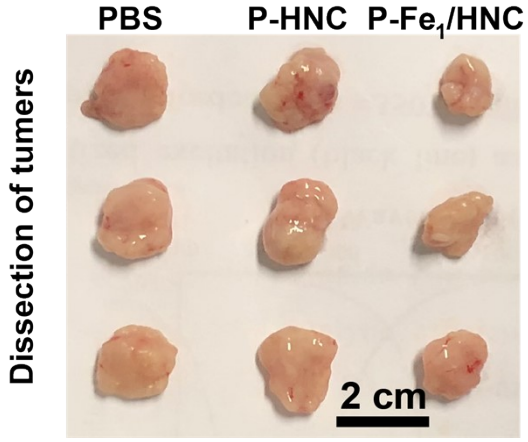

Fig. S29 Digital photographs of dissected tumors from the groups treated with PBS, P-HNC and P-Fe_1/HNC, respectively.

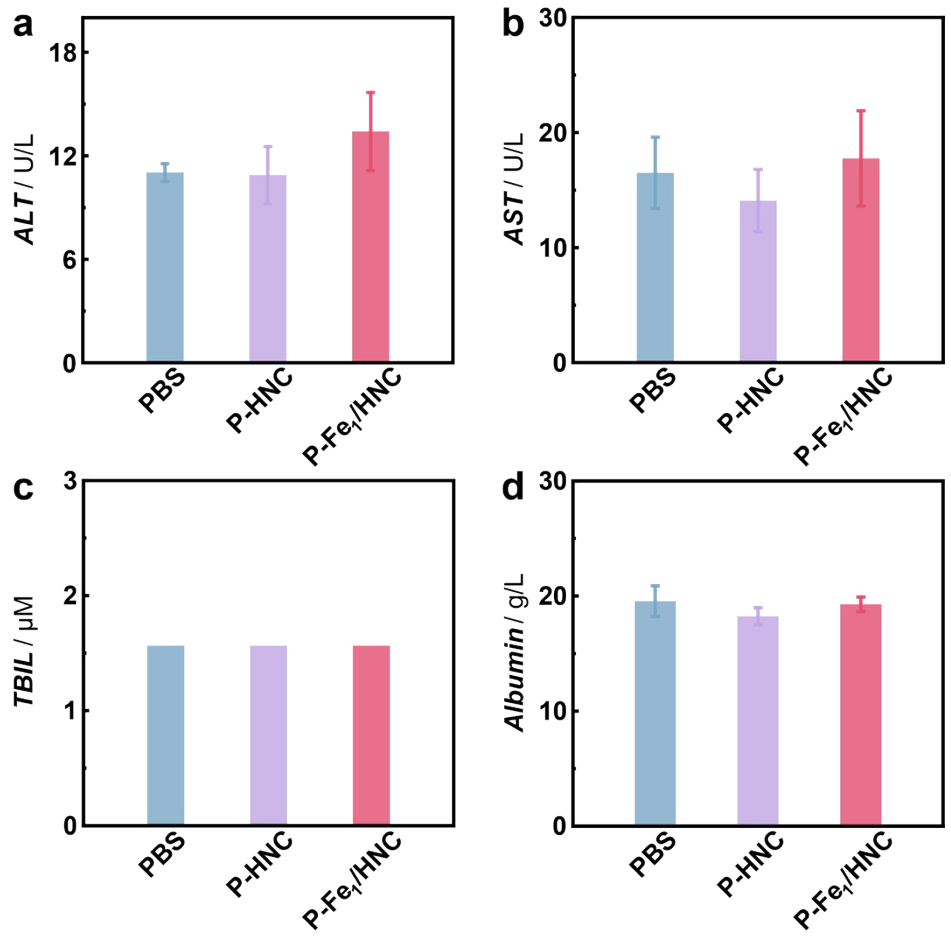

Fig. S30 Blood biochemical analysis of (a) ALT, (b) AST, (c) TBIL and (d) Albumin for P-Fe_1/HNC treated mice.